Clean Energy, 2024, Vol. 8, No. 3, 127–135
https://doi.org/10.1093/ce/zkae030
Advance access publication 25 April 2024
Engineering Practice

Technological parameters of thin-film pulsed laser scribing for perovskite photovoltaics

Rustam Ishteev[1,2,*], Pavel Gostishchev[2,3], Mariia Tiukhova[3], Anton Sorokin[1], Arthur Ishteev[2,3,4], and Vladimir Kondratenko[1]

[1]Laboratory of Precision Machining of Materials, Department of Nanoelectronics, Institute for Advanced Technologies and Industrial Programming, RTU MIREA, Moscow, Russia
[2]Research and Practical Clinical Center for Diagnostics and Telemedicine Technologies of the Moscow Health Care Department, Moscow, Russia
[3]Laboratory of Advanced Solar Energy (LASE), National University of Science and Technology MISIS, 4 Leninsky St., Moscow, Russia
[4]Semenov Federal Research Center of Chemical Physics, Russian Academy of Sciences (RAS), 4 Kosygina str., Moscow, Russia
[*]Corresponding author. E-mail: rustamishteev@gmail.com

Abstract

Over the past decade, the power conversion efficiency of halide perovskite solar cells has shown a rapid increase to 26.1%. The significant efficiency growth and the relative simplification of the technology for obtaining thin-film solar cells due to liquid printing methods determine the high potential for the low-cost perovskite solar cells manufacturing. However, efficient use of cell geometry is comparable to the size of standard crystalline-Si wafers (156:156 mm and more). Therefore, modular geometry similar to amorphous-Si solar cell approaches is used to scale perovskite solar cells. Serial electrical connection of thin-film cells requires precise processing of the conductive layers that form the device p-i-n structure. The subject of research is the development of a full pulsed laser scribing cycle for inverted perovskite solar cells. In this work, we propose a study of a laser-patterning technology In_2O_3:SnO_2 (ITO) conductive layer and a photoactive perovskite layer $Cs_{0,2}(CH(NH_2)_2)_{0,8}PbI_3$. Process regimes of transparent conducting electrodes based on ITO and halide perovskite layer $Cs_{0,2}(CH(NH_2)_2)_{0,8}PbI_3$ laser patterning were obtained. The optimal parameters for the multipass mode processing of ITO and perovskite layer were determined. The cell was electrically isolated at a scribe line width of 30 μm.

Graphical Abstract

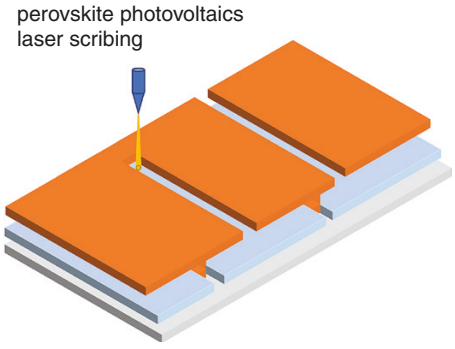

Keywords: patterning; perovskite; solar cell; perovskite solar cell; photovoltaics; scribing

Introduction

Perovskite solar cells (PSCs) have shown great potential for high-efficiency and low-cost solar power generation. Halide perovskites exhibit high absorption coefficient in the visible spectral range [1], high defect tolerance [2], radiation resistance [3], tunable band-gap width in the range of 1.16–3.04 eV [4] and high charge-carrier mobility (10–100 $cm^2/(V{\cdot}s)$) [5, 6]. These characteristics make halide perovskites a promising material for solar energy absorption.

Perovskite thin films are positioned between planar top and bottom electrodes, with p-i-n and n-i-p configurations in which the perovskite acts as the photoabsorber and is deposited on a substrate between a hole-transport and electron-transport layers. The bottom electrode can be made of transparent conductive In_2O_3:SnO_2 (ITO), while the top is usually a metal that forms an ohmic contact with the charge-transport layer (Ag, Cu, Au, etc.).

Perovskite-based thin-film solar cells have gained significant attention in the scientific community due to their low capital cost and high performance (26.1% power conversion efficiency) [7] comparable to commercial silicon-based solar cells. This presents an opportunity for PSCs to become a commercially viable renewable energy source. Researchers are working on adapting

Received: 19 October 2023. **Accepted:** 21 March 2024

laboratory technologies to meet industrial production standards and scaling up perovskite photoconverters is an important step towards commercialization [8].

Laser scribing is one of the key industrial methods for patterning thin-film optoelectronic devices [9–11]. The continuous CO_2 laser can be successfully used to pattern transparent conductive oxides. The intraband absorption of free carriers allows the effective ablation of wide-band-gap materials using an infrared laser (emission wavelength = 10.6 um) [12]. The use of CO_2 for the ablation of ITO demonstrated relevant results, even for flexible thin-film substrates [13]. However, the continuous mode of the CO_2 laser led to thermal damage in the scribed area. Nanosecond lasers provide a high degree of flexibility in altering the pulse duration and emission wavelength [14]. Femtosecond lasers operate with extremely short pulse durations in the range of 10^{-15} s. This enables precise material processing with minimal heat generation, allowing high-quality scribing with reduced collateral damage, which is particularly suitable for processing heat-sensitive materials [15]. However, the utilization of femtosecond laser scribers typically involves higher costs compared with other types of lasers and limits the patterning of thick multilayer structures. Patterning of PSCs using laser ablation requires alignment of various approaches. The technological process of scribing thin-film devices based on halide perovskites involves the sequential ablation of wide-band-gap oxide materials and metal–organic films. The layer-by-layer ablation of the material necessitates the optimization of laser beam power, speed and depth penetration.

Our study provides a comprehensive comparison of the use of different ablation approaches with continuous and pulsed lasers. This broad approach allows us to provide a detailed comparison of the effects of different laser regimes on the quality of scribing and the subsequent performance of the solar cells. We have optimized the scribing parameters for each type of laser, achieving control over the scribing process, minimizing damage to the substrate and ensuring the integrity of the photovoltaic layers.

Notably, the current manufacturing processes for PSCs are still focused on research purposes. In order to make a step towards industrial production, perovskite devices need to be upscaled. The scaling of laboratory sample areas (up to 1 cm^2) increases the resistance losses in the thin conductive layers of the semiconductor structure. In particular, losses occur at the ITO electrode. The surface resistivity, length and width of the conductive layer (Equation (1)) have an influence:

$$\mathrm{SR}\,[\,\Omega\,/\square] = \mathrm{R}\,[\,\Omega\,] \cdot \frac{L\,[m]}{W\,[m]}, \tag{1}$$

where $\mathrm{SR}\,[\,\Omega\,/\square]$ represents the surface resistance of the layer, $\mathrm{R}\,[\,\Omega\,]$ represents the resistance, $L\,[m]$ represents the layer length and $W\,[m]$ represents the layer width.

In the realm of thin-film solar cell technology, the optimization of sheet resistance through laser scribing stands as a critical factor in enhancing power conversion efficiency (PCE) and ensuring module reliability. The sheet resistance (SR), defined by the Equation (1), plays a pivotal role in determining the series resistance of the solar cell and thereby energy losses to scaling of the solar cell.

Typically, upscaling PSCs to modules is achieved by in-series connection. The lateral dimensions of pixels reach units of tens of centimetres. The standard transparent conducting electrode in perovskite photovoltaics is ITO, characterized by SR values ranging from ~10^0 Ω/□. Current collections from a large-area ITO electrode can be affected by resistive losses. An increase in the contact resistance (also called series resistance) of a solar cell can reduce the maximum power of PSCs. The task of PSC cell design and patterning is important for improving device performance.

On the way towards the upscaling of solar cells, elevated SR increases the series resistance of the solar cell, which is detrimental to its performance. This increased series resistance steepens the slope near the length of the current–voltage (*I*–*V*) curve, effectively reducing the area under the curve. Since the area of the device depends on the charge travel length, a higher SR translates directly into lower energy conversion efficiency.

Laser scribing addresses this challenge by precisely segmenting the solar cell, thereby reducing the length (*L*) of the conductive path. This reduction in length diminishes the SR, leading to a lower series resistance. The result is an optimized *I*–*V* curve with a less steep slope at the X-intercept, enhancing the PCE of the solar cell.

Beyond improving efficiency, laser scribing plays a crucial role in segmenting the solar cell into smaller sections. This segmentation is key in the event of a short circuit in one segment; it ensures that the overall module continues to operate with only a marginal reduction in power output. This segmentation thus not only enhances the efficiency of individual cells, but also significantly increases the resilience and reliability of the entire solar module [9, 10, 16].

The patterning is realized by successive scribing steps with a parallel offset to the preceding cut, so that the layers form a consistent cell connection in the module (Fig. 1). Each of the processes is denoted as P1—bottom electrode scribing, P2—semiconductor components scribing and P3—top electrode scribing [17–19]. Technological alternatives to scribing are bus brazing of small-sized single elements, chemical etching and mechanical scribing. However, such methods have significant disadvantages, reducing the effective area of the photoactive cell and inhomogeneous removal of cutting products, therefore reducing the output characteristics of the module.

Overall, the use of laser technology in the production of PSCs and modules has the potential to significantly improve their efficiency, stability and cost-effectiveness. As such, Brooks *et al.* discuss that it is an area of active research and development in the solar industry [20].

The process parameters used during laser patterning play a crucial role in determining the quality of the final device. Factors such as laser wavelength, pulse duration and fluence all affect the ablation properties of the material. Essentially, the wavelength of the laser dictates which layers can be removed, since it depends on the optical absorption of the material. Meanwhile, the fluence and pulse duration determine the ablation rate and thermal impact on the material.

When it comes to producing high-quality scribes, P1 and P3 scribes require a large isolation resistance across the scribed line. In contrast, successful P2 patterning is characterized by low series

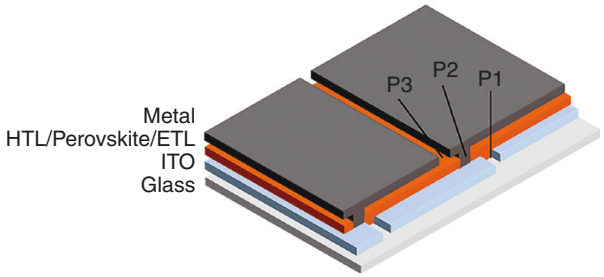

Fig. 1: Scheme of a perovskite solar module with fragmented layers

resistances, which can be achieved through a clean and smooth bottom of the scribed line. By taking all these factors into account and optimizing the process parameters, Schultz *et al.* show that manufacturers can produce laser-patterned products that meet their desired specifications [21].

The use of a nanosecond 1064-nm laser has been shown by Teng *et al.*. The use of this type of laser demonstrated 13.1% module efficiency, but the use of this wavelength is not optimal for perovskite technologies, as demonstrated by the high contact resistance of the resulting devices. In a paper by Lin *et al.* [22], the authors demonstrated the use of a 532-nm nanosecond pulsed laser to perform all scribing processes (P1–P3) to produce translucent perovskite solar mini-modules with an efficiency of 12.5%. Gao *et al.* were able to achieve an efficiency of 21.07% and a geometric fill factor of 95.5% when creating perovskite modules using a nanosecond laser, demonstrating that nanosecond lasers can be used to create high-performance devices. The advantages of nanosecond lasers over picosecond or femtosecond lasers are their high stability and low cost, and therefore they are applicable to large-scale production of perovskite solar modules [23].

Zhao *et al.* [24] have shown that the use of picosecond and femtosecond lasers holds great promise, as unwanted thermal effects are significantly reduced and localized. This makes it possible to remove the metal electrode, hole-transport layer and perovskite without causing thermal degradation. As a result, they have been able to achieve a champion efficiency of 17.5% and 9.1% on 5:5 cm fabricated perovskite modules via femtosecond laser direct writing. Wang *et al.* showed that they were able to create perovskite modules with a high level of PCE (16.65%) and geometric fill factor (98%) using a femtosecond laser with a 1030-nm wavelength, which demonstrates the advantages of pico- and femtosecond lasers in the precision of scribing different materials [25].

Laser wavelength is an important factor for perovskite solar module scribing processes. Each of the P1–P3 steps requires a specific wavelength, depending on the materials to be removed. Infrared (IR) lasers can be used to scribe the translucent electrode and metal contact in steps P1 and P3. However, the use of IR lasers thermalizes areas near the cut and can cause damage to the ITO cut boundary regions during the P1 process and photoactive layers sensitive to high temperature during P3. In the case of ultrashort ultraviolet (UV) laser pulses, the peak power of the pulse excites material atoms that acquire sufficient energy to break lattice bonds or molecular structure. They are instantly broken before they have time to transfer their energy to neighbouring lattice atoms and there is a direct transition from solid to vapour without damaging or heating the area near the cut.

Also, the use of IR lasers is not applicable for the P2 stage, since perovskite and transport layers do not absorb the IR spectrum and laser radiation will affect the lower translucent electrode, causing thermalization and damage to the entire solar cell structure. For the P2 step, lasers with wavelengths in the visible and UV bands are needed. Visible-spectrum lasers may not be effective with wide-area perovskites and transport layers. In contrast, UV lasers are versatile tools for all stages of perovskite solar module scribing, regardless of the device configuration and material combination.

In this work, we studied the technological regimes of ITO film and $Cs_{0,2}(CH(NH_2)_2)_{0,8}PbI_3$ perovskite removal using the most-distributed industrial-standard laser from display manufacturing. A widely affordable multipurpose CO_2 gas laser (Sinrad 48-5), a more advanced UV nanosecond pulsed laser (MPL 01-106-355) and advanced femtosecond TETA-10 lasers were used for the study.

The infrared gas laser stands as a robust and cost-effective solution. Its primary advantage lies in its affordability and widespread availability in industrial settings. The longer wavelength of the CO_2 laser facilitates efficient absorption by a wide range of materials, making it particularly suitable for scribing ITO films. The CO_2 laser imparts a significant amount of heat into the substrate, which can lead to thermal damage in sensitive materials such as perovskite.

The cost of nanosecond UV lasers and their operational complexity are generally higher than those of CO_2 lasers, which may be a limiting factor for widespread adoption in cost-sensitive manufacturing environments. The NANIO-355 ultraviolet laser built into the MPL 01-1060-355 set-up operates at a wavelength of 355 nm, maximum pulse frequency of 100 kHz, radiation power of 3.8 W and single-pulse duration of 40 ns. The shorter pulse duration and higher photon energy inherent in UV lasers allow precise ablation of material with reduced heat-affected zones. This precision is particularly advantageous in creating the intricate patterns necessary for advanced thin-film scribing application.

The technical characteristics of the femtosecond laser are as follows: maximum radiation power of 10 W, maximum pulse frequency of 200 kHz, pulse duration of 250 fs, radiation wavelength of 1030 nm.

The Sinrad 48-5 CO_2 gas laser specifications are as follows: pumping type continuous radiation, wavelength of 10.6 μm.

The result of the work is the technology for patterning perovskite solar module components by the laser scribing of an ITO electrode and halide perovskite $Cs_{0,2}(CH(NH_2)_2)_{0,8}PbI_3$ on glass substrates. The proposed technology provides a cutting width of ≤25 μm and a solar cell operability of 18%.

The CO_2 gas laser and the UV nanosecond laser are part of a single MLP1-1060/355 machine, which is used for crystal cutting technology by laser-guided thermal splintering (GTS) [26]. GTS technology is designed to cleave brittle non-metallic materials such as silicon and sapphire wafers. The principle of its operation is based on heating the material using a laser beam along the cutting line and the subsequent cooling of the heated area using a refrigerant. Due to this technology, microcracks are formed in the materials, which split the material without microdefects. The laser beam is slightly extended in the direction of the cutting axis at the output of the lens. The cutting of ITO and perovskite films with the two presented lasers demonstrated that, for the ITO film processing, the CO_2 laser is promising; as for perovskite film, the UV nanosecond laser is prospective. While cutting the perovskite film with the CO_2 laser, partial surface destruction of the adjacent ITO film was observed and the UV nanosecond laser demonstrated minor film removal when cutting the ITO film.

Also, the cutting modes of the ITO film were investigated on a TETA-10 femtosecond laser, which was provided by the company ESTO. This laser is used for the precision processing of various materials.

1 Fragmentation of perovskite solar module components

The surface area bounded by lines P1 and P3 is not photogenerative. It is essential is to minimize it by thinning the scribing lines and positioning the cutting lines accurately.

The P1 process provides complete isolation of adjacent areas of the 220-nm-thick ITO layer on the glass substrate. The glass surface should not have any cracks, grooves or elevations, as these can cause the upper and lower electrodes to be short-circuited.

Next, semiconductor layers are applied to the substrate to form a p-i-n structure, including a 450-nm-thick perovskite layer. A metal layer is then applied as the top electrode. The top and bottom electrodes of each cell are short-circuited by P2 forming a series connection. The P2 process forms a cut in the perovskite layer to provide a connection between the ITO anode and the metal cathode without damaging the bottom electrode.

The P3 process is a 100-nm-thick patterning of the top electrode and has been replaced in this work by stencil-mask deposition to increase the reproducibility of the experiment.

2 Materials

To determine the optimum parameters for laser scribing of the ITO film (P1 process), commercially available glass substrates used in the production of solar cells and organic light-emitting diodes (LEDs) are employed in this study. The substrates are 1.1 mm thick with a 2.5-nm SiO_2 barrier layer and a 220-nm-thick In_2O_3:SnO_2 conductive coating from Kaivo (R_{sheet} resistance 7 Ω/□, light transmission 77%).

Further, the laser treatment regimens of the perovskite layers on the surface of the ITO-coated–P2 substrates were investigated. In this work, the perovskite films (PFs) were obtained by using centrifugation from a solution of $CH(NH_2)_2I$, CsI and PbI_2 salts in a dimethyl sulfoxide (DMSO) and dimethylformamide (DMF) solvent mixture. Crystallization of the PF was carried out by exposure to an antisolvent[12] followed by an annealing at 105°C. Absorption and photoluminescence (PL) spectra were measured to determine the optical properties of the PF (Fig. S1 in the online Supplementary Data). In accordance with the obtained results, the light absorption of the perovskite $Cs_{0,2}(CH(NH_2)_2)_{0,8}PbI_3$ was determined in the spectral range from 600 to 850 nm and the PL peak was observed at 790 nm. The strong optical absorption of $Cs_{0,2}(CH(NH_2)_2)_{0,8}PbI_3$ in the UV range and total light transmission in the IR spectrum cause the choice of laser for treatment of the P2 configuration with wavelength 350 nm [27].

To verify the performance of the proposed scribing technology for a perovskite solar cell on a glass substrate, a device with the following structure was fabricated: ITO/NiO_x/ $Cs_{0,2}(CH(NH_2)_2)_{0,8}PbI_3$/C60/BCP/Ag with a fragmented ITO layer (process P1). A detailed description of the device manufacturing is described in the work [28]. Since, at this stage, only the laser modes in the P1 and the patterning processes of the perovskite film (P2 process) were investigated, the metal electrodes (P3 process) were replaced by sputtering of the electrode through a mask [20].

The study of the laser-patterning of the ITO film (P1 process) was carried out with CO_2 and femtosecond lasers.

2.1 Fragmentation of ITO film using a CO_2 laser

Circle diameters of 4 mm were cut out on the surface of the ITO film using different laser processing modes. A circular line was used to define the insulated area inside the circles and evaluate the insulating ability of the scribes on the conductive ITO film. The cutting modes for the nanosecond laser were set in a laser pump power range from 1.2 to 2.5 W. The substrate movement speed ranged from 20 to 50 mm/s with a step of 5 mm/s and a single pass was plotted for each circle. First, we made a raw selection of modes that excluded glass cracking by optical evaluation with an upright microscope. The optical images of the cut lines are presented in Table S1 (see the online Supplementary Data). Second, we evaluated the insulation across the cutting line. The electrode probes of the resistance meter were placed in and out of the circle to measure the resistance and select the insulated scribes (Table S2 in the online Supplementary Data). Among all combinations of velocity and power, the single-pass mode achieved full isolation in the power range of >1.5 W with a processing velocity from 35 to 45 mm/s.

Further increases in the radiation power provided complete isolation of the patterned areas but produced microcracks (Table S1 in the online Supplementary Data, power range > 2 W). At lower power values, incomplete isolation of the ITO conductive areas was observed (Table S2 in the online Supplementary Data).

Table S1 in the online Supplementary Data shows the results obtained in the single-pass cutting mode, which scans the surface of the material in one iteration.

Furthermore, multipass cutting modes were used in the study. There are multiple scanning cycles performed in these methods. The multipass modes were two-pass, three-pass and five-pass.

In order to optimize the patching technology of the ITO film (P1 process) using the CO_2 laser, a multipass mode (two-pass mode) of cutting with 1.5 W of power was applied and the cutting speed was increased to 100 mm/s. A lower power of radiation does not provide isolation, while increasing this parameter mostly causes damage to the substrates. This regime was precisely investigated by using scanning electron microscopy (SEM) and atomic-force microscopy (AFM). A nonconductive ('dead') zone width of ≤25.38 μm is achieved (Fig. 2b) for the two-pass mode. An assessment of the scribed area isolation quality is demonstrated by the charge collection inside the circle on SEM contrast imaging (Fig. 2d). Since the circle area is fully isolated, there is no drain for the electrons from electron-beam accumulation to leak out of the circle. The profile of the scribed path has a 100-nm-high hail that was detected along the edge line (Fig. 2c). The hail height exceeded the desired threshold as it could cause a short circuit between the upper and lower electrodes, and consequently reduce the output performance of the device (Fig. 2c). Fig. 2d demonstrates the isolated region.

Fig. 2a shows the patterning scheme of the ITO film. Fig. 2b illustrates the ITO film-cutting line using a two-pass method at 1.5 W of radiation power and a cutting velocity of 100 mm/s. This mode causes the removal of the entire ITO film and the integrity of the glass substrate. The hail height along the edge is 100 nm (Fig. 2c), which prevents the charge flow in the series-connected cells of the solar module and leads to short-circuited devices. Experimentally, it was found that, at emission powers of <3 W, the CO_2 laser does not support the set emission precisely, as spontaneous emission can occur in these cutting modes (Tables S1 and S2 in the online Supplementary Data).

2.2 Fragmentation of ITO film using a femtosecond laser

The femtosecond laser has an advantage for P1 (ITO scribing) processes, as it is the most efficient, but it is also a less affordable method. A variety of femtosecond laser regimes were tested for the P1 process. The range of radiation power at the lens output was from 0.14 to 0.68 W at a pulse frequency of 100 kHz. The range of laser velocity relative to the substrate was 166–500 mm/s with steps of 83 mm/s. The maximum power of the femtosecond laser is limited to 0.68 W. Higher power damages the glass substrate for the whole variety of velocities. The essential problem

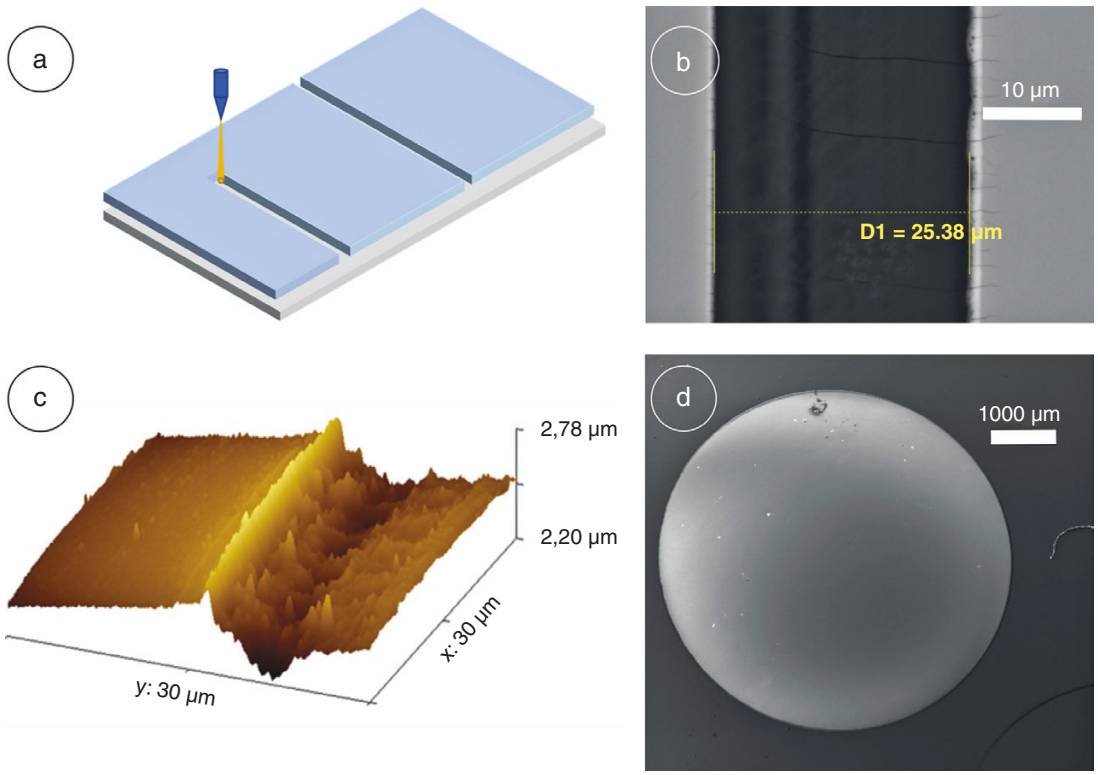

Fig. 2: ITO film patterning using a CO_2 laser. (a) ITO film patterning scheme; (b) cutting line using the two-pass mode: velocity 100 mm/s, radiation power 1.5 W; (c) study of the two-pass mode using an atomic-force microscope; (d) SEM contrast image of isolated ITO area.

is to minimize the hail on the cutting line edges. Hails were measured by using the AFM method (Figure S3a in the online Supplementary Data).

At a radiation power of 0.14 W (Figure S2a in the online Supplementary Data), incomplete penetration of the laser beam into the ITO layer was demonstrated. No change in the surface resistance of the film was observed in this mode of treatment. Removal of sections of the ITO layer with preservation of the integrity of adjacent areas is demonstrated at a radiation power of 0.29 W (Fig. S2b in the online Supplementary Data). Removal of the ITO layer throughout the entire depth with the formation of defects on the glass substrate is shown at an irradiation power of 0.68 W (Fig. S2c in the online Supplementary Data). The radiation power of 0.29 W was further considered in the multipass treatment mode.

Two-pass and three-pass treatment modes were performed. Each successive line in the multipass mode was processed in increments of 3–4 μm. To eliminate the occurrence of further defects in the form of hail on the surface of the ITO film, it was proposed to increase the processing velocity to 416 mm/s to reduce the exposure time of laser radiation on the surface of the glass substrate.

The optimal ITO film-cutting modes were demonstrated by the three-pass and hybrid-pass cutting modes (Fig. S3b and S3c, respectively, in the online Supplementary Data), as they showed the required insulating characteristics of adjacent ITO layers; the hail height was 50 nm (Fig. 3a). This number is satisfactory for the P1 process since the ITO hail is less than the perovskite layer thickness (500 nm) and this minimizes the chance of pinning the top electrode and shorting the entire solar module. We propose a hybrid-pass mode that first uses a three-pass mode at 0.29 W and then a two-pass mode at 0.14 W to remove the remaining hail formed during the three-pass operation. The hail heights of this cutting method were 20 and 30 nm on each edge along the entire scribe and the width of the 'dead area' was ~25 μm. The three-pass mode (Fig. 3a) demonstrated hail heights of 40 and 50 nm on each edge of the selvedge. The scribe width in this machining mode was 20 μm. Fig. 3b demonstrates the result of cutting with a hybrid (five-pass) mode. This process consists of removing the ITO layer using a three-pass cutting mode with 0.29 W of laser power at a cutting speed of 416 mm/s, followed by a two-pass cutting mode with 0.14 W of laser power at a cutting speed of 416 mm/s to remove the hail on the surface.

2.3 Fragmentation of perovskite film (P2) using a UV nanosecond laser

To determine the parameters of the laser-patterning mode for the perovskite layer in the cutting mode of the P2 process using the more affordable UV nanosecond pulsed laser, we tested the range of radiation powers from 0.3 to 0.8 W in increments of 0.1 W. The processing velocity range was 80–120 mm/s in 5-mm/s increments. The perovskite layer was patterned on a glass substrate with an ITO layer (Fig. 4a). Cuts in which no traces of perovskite were observed at ×100 optical magnification, the integrity of the preceding layers was retained and the cut width was minimal were evaluated as relevant (Table S3 in the online Supplementary Data). A relevant machining result was obtained at a radiation power of 0.4 W at a velocity of 110 mm/s (Fig. 4b) with a 'dead zone' width of 17 μm.

Modes with a treatment rate of <80 mm/s showed surface destruction of the adjacent ITO layer structure. At a processing velocity of 115 mm/s and a power of 0.3 W, the minimum width of the 'dead zone' was 22.1 μm but, due to the pulse mode of laser operation at high spot movement velocity, torn edges of

the cutting line were observed. When the power was increased to 0.5 W, the 'dead zone' widened to 28.4 μm. With a processing velocity of >115 mm/s, regulation of the 'dead zone' becomes complicated, as the pulse laser mode leaves jagged edges of the cutting line at a radiation power of 0.4 W and expands the cutting line as the radiation power increases. A re-examination of the laser-patterning modes of the perovskite layer confirmed the previous research [28].

Using a processing velocity of 110 mm/s and a radiation power of <0.4 W, partial removal of the perovskite layer along the cutting line was observed, preventing consistent cell connection after application of the metal electrode. Reducing the velocity to 105 mm/s at a cutting power of 0.3 W demonstrated a widening of the 'dead zone' to 26.1 μm and partial removal of the perovskite layer. A table of results for the perovskite patching modes is presented in Table S3 in the online Supplementary Data.

The 0.4 W–110 mm/s mode provided optimum depth and width of cut, and was examined by using SEM (Fig. 4b and c). The 0.4-W radiation power and 110-mm/s machining velocity mode demonstrated the integrity of the adjacent ITO layer structure, complete

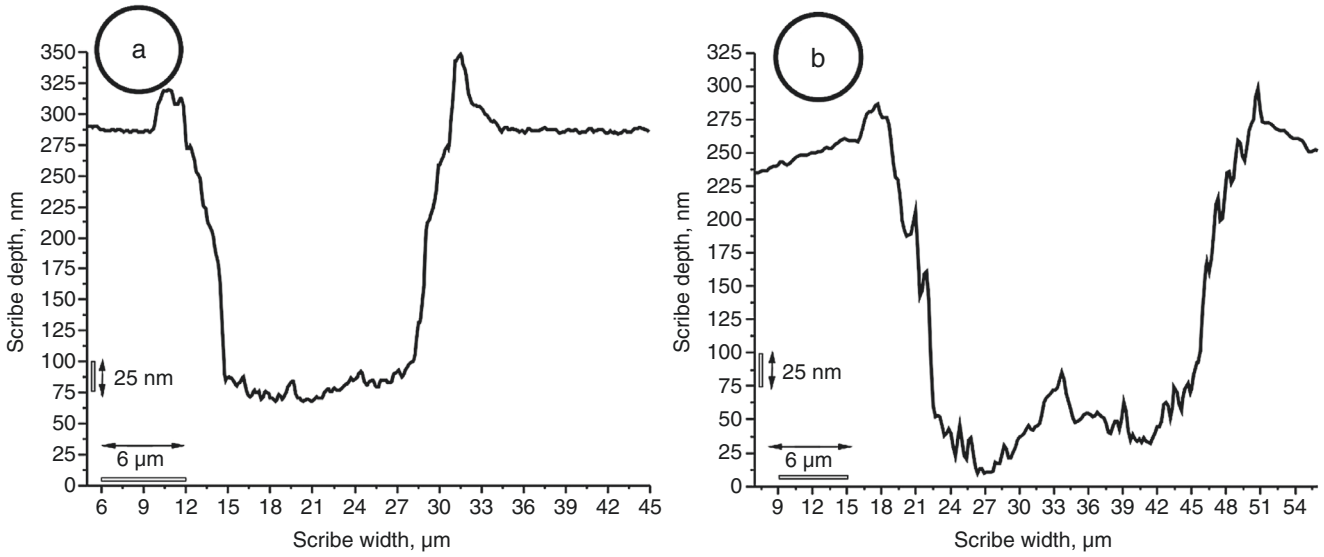

Fig. 3: Profilometry of scribes after patching of the ITO layer using a femtosecond laser. (a) Three-pass cutting with 0.29 W of radiation power at a cutting velocity of 416 mm/s; (b) hybrid-pass (five-pass) mode.

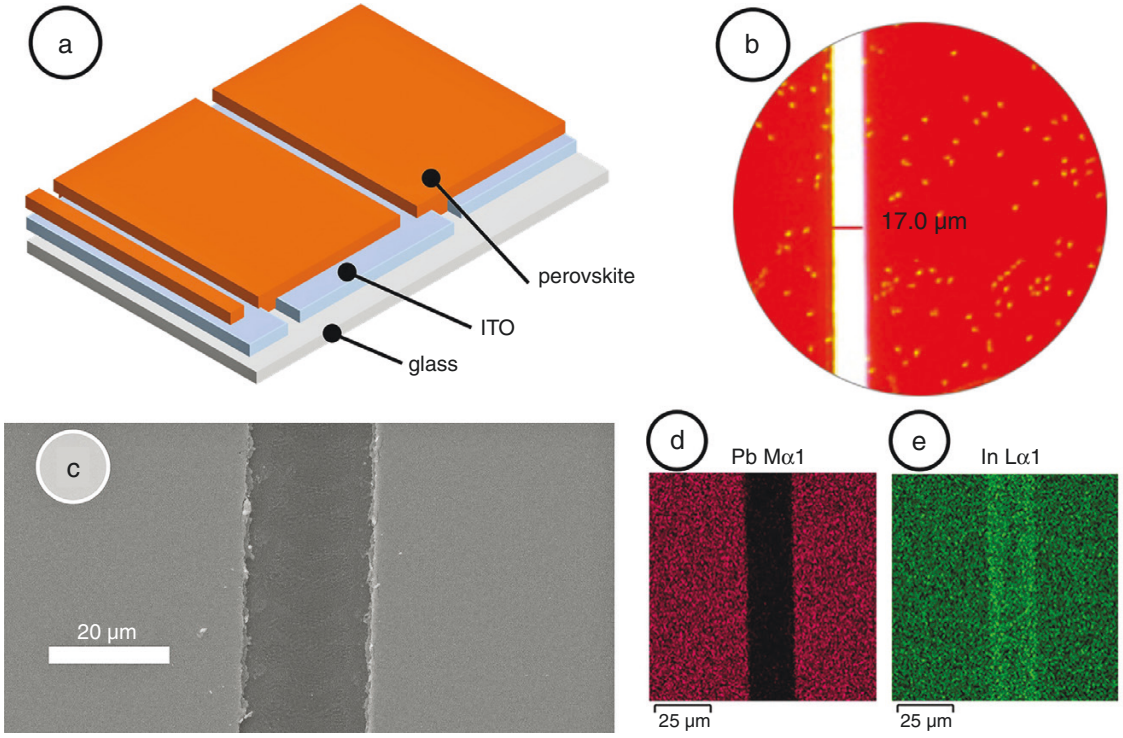

Fig. 4: Patterning of the perovskite layer. (a) Perovskite patterning scheme (P2); imaging of cutting line using a nanosecond UV laser at power of 0.4 W, processing velocity of 110 mm/s and focus raised + 200 μm; (b) optical; (c) SEM image; (d) EDX mapping for In as a component of ITO under the cutting line.

removal of the perovskite layer along the entire machining line and the smallest 'dead zone' width.

Further refinement involved SEM imaging combined with Energy Dispersive X-ray (EDX) spectroscopy. This analysis allowed us to assess the presence of elements from the ITO layer (Sn and In) and the absence of perovskite constituents (Cs and Pb) along the scribed line. In the same power setting of 0.4 W but across a broader velocity range (105–115 mm/s), we observed gaps in the Sn and In mapping at higher velocities (113 and 115 mm/s), indicating less damage to the ITO layer (Table S4 in the online Supplementary Data).

To overcome this challenge, we reduced the laser power and raised the focus to 200 µm, while examining the same range of velocities (Table S5 in the online Supplementary Data). This adjustment resulted in unbroken Sn and In layers across all velocities, with a clear and complete removal of Pb and Cs, indicative of an effective scribing process (Fig. 4e).

Finally, we explored a three-pass mode with the laser power set to 0.4 W and focus increased to 250 µm to dilute the power density on the light spot (Table S6 in the online Supplementary Data). This was tested across the velocity range of 105–115 mm/s. The optimal results were obtained at a velocity of 107 mm/s, at which no traces of Pb and Cs were detected on the scribe line and the ITO layer remained undamaged (Fig. 4d and e). Higher velocities in this mode resulted in incomplete removal of the perovskite layer.

The optimal regime for the P2 process (Fig. 4a), ensuring complete removal of the perovskite layer while preserving the ITO layer, was achieved with a laser power of 0.3–0.4 W, a focus raised to 200–250 µm and a velocity of 107 mm/s in a three-pass mode. This regime guarantees the precision required for high-efficiency PSCs, balancing the delicate interplay between complete perovskite removal and ITO layer preservation.

2.4 Influence of laser scribing parameters on the device characteristics of thin-film photomodules

To approve the results, solar cells based on iodine perovskite ($Cs_{0,2}(CH(NH_2)_2)_{0,8}PbI_3$) were fabricated with multipass modes patching the ITO film using a femtosecond laser. To reduce the risks of reproducibility failure, the fragmentation lines of the metal electrode were evaporated onto the device through a mask. The performance of the PSCs based on $Cs_{0,2}(CH(NH_2)_2)_{0,8}PbI_3$ was evaluated by comparing the open-current voltage U_{oc}, short-circuit current density J_{sc} and fill factor (*FF*) between the two-, three- and five-pass methods (scribe profiles and optimization process are presented in Tables S4–S7, respectively, in the online Supplementary Data). The difference between the two-, three- and five-pass modes is the number of additional iterations of laser treatment of the material. For the two-pass mode, the laser beam is displaced by 4–6 µm from the first iteration for the second cut. For the three-pass mode, the second and the third cutting lines are shifted in opposite directions from the first cutting by 4–6 µm. For the five-pass (hybrid-pass) mode, the cutting pattern is identical but the last two lines are performed with an offset of 4–6 µm from the edge of the cutting lines after the three-pass mode. The difference between the two-, three- and five-pass modes is the number of additional iterations of laser treatment of the material. For the two-pass mode, the laser beam is displaced by 4–6 µm from the first iteration for the second cut. For the three-pass mode, the second and the third cutting lines are shifted in opposite directions from the first cutting by 4–6 µm. For the five-pass mode, the cutting pattern is identical but the last two lines are performed with an offset of 4–6 µm from the edge of the cutting lines after the three-pass mode.

The *I–V* characteristics of the PSCs were measured by using a Keithley 2400 source-meter with a voltage sweep in the range of 0–1.3 V. The devices were connected by clamping contacts to the ITO anode and to the silver cathode (Fig. 1). The measurements were made using a solar simulator under conditions of AM 1.5 G, which corresponds to a light intensity of 100 mW/cm^2 and the solar spectrum.

PCEs were calculated using Equation (2). The output characteristics of the devices are given in Table 1.

$$\eta = \frac{J_{sc} \cdot U_{oc} \cdot FF}{P_{in}}, \tag{2}$$

where η represents the PCE (%), P_{in} represents the intensity of the incident light (mW/cm^2), J_{sc} represents the short-circuit current density (mA/cm^2), U_{oc} represents the open-current voltage (V) and *FF* represents the fill factor (%).

The output performance of the reference device (chemical etching, no laser scribing) was V, mA/cm^2, FF and PCE.

The open-circuit voltage of the devices in all of the ITO film processing methods is relatively the same (1–1.03 V) (Table 1). The three-pass mode showed the maximum current density (26.43 mA/cm^2) but the FF deteriorated (67.98%). Three-pass treatment at 0.29 W followed by two-pass treatment at 0.14 W showed a 3-mA/cm^2 (hybrid-pass) lower short-circuit current than the three-pass mode, 0.5% lower PCE than the three-pass mode and 6% higher FF than the three-pass mode.

The open-circuit voltage of the three-pass treatment mode is 0.03 V lower than that of the five-pass mode. At the same time, the short-circuit current of the three-pass ITO film processing mode device is higher by 3.4 mA/cm^2. In terms of FF and PCE, the devices are comparable and differ by 3–6% and 1%, respectively.

The highest performance, with a PCE of 18.04%, was obtained on a device in which the ITO film removal was realized using a femtosecond laser. A perovskite solar cell with the same cell size on a 25 × 25 mm substrate without the use of laser scribing was fabricated as a reference. This solar cell showed a PCE of 18%, which is identical to that of the sample tested.

The output characteristics of the photoconverters using femtosecond laser processing of the ITO film are shown in Fig. 5.

The *I–V* curves of the devices in the three-pass mode compared with a combination of the three-pass mode with 0.29 W of radiation power and the two-pass mode with 0.14 W of radiation power are 0.5% higher in PCE and 2.67% lower in FF.

The shunt and series resistances in the PSCs significantly determine the FF, which is largely influenced by the quality of the contacts. Hence, the optimum processing mode is a combination of a three-pass and then a two-pass mode with less radiation power. This is aimed at removing the generated fouling after the three-pass cutting mode. In this case, the hail heights are 20 and 30 µm (Fig. 3b), which is lower than the three-pass mode with a hail height of 40–50 nm.

Table 1: Output characteristics of perovskite solar cells with different methods of ITO film processing using a femtosecond laser

ITO film fragmentation methods	U_{oc} (V)	J_{sc} (mA/cm^2)	FF (%)	PCE (%)
Three-pass	1.00	–26.43	67.98	18.04
Hybrid-pass	1.03	–23.16	73.68	17.54

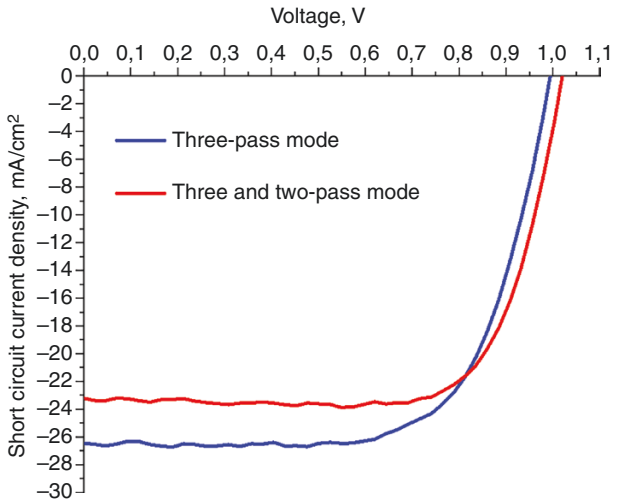

Fig. 5: Output characteristics of the device with ITO film treatment using a femtosecond laser

3 Conclusion

In this work, laser fragmentation modes for perovskite and ITO films were determined. A femtosecond laser showed the best processing quality of ITO film in comparison with a nanosecond laser. The optimum method for processing ITO films using a 1030-nm femtosecond laser is a combination of the three-pass mode with 0.29 W of radiation power and the two-pass mode with 0.14 W of laser power at laser beam scanning velocity of 416 mm/s. Fabricated PSCs showed a maximum FF of 73.68% and a maximum PCE of 17.5%. At these parameters, the hail height was 20 and 30 nm at the cutting line edges. The width of the patterned line was 19 μm. A power of 0.29 W was used for femtosecond laser treatment of the ITO film while 1.5 W was required for nanosecond laser treatment of the same surface. It proves that the parameters defined in this work for the femtosecond laser are not applicable to lasers with other radiation intensities.

The perovskite layer was removed using a nanosecond laser at 0.4 W. While treating the perovskite film using a nanosecond laser, a power close to the value of the excitation initiation of the laser radiation should be used whilst at the same time not causing spontaneous excitations leading to non-uniform intensity of radiation along the whole scanning line. Treatment of PFs using a femtosecond laser at a wavelength of 1030 nm is not possible due to the reduced absorption coefficient of the material in the infrared region of the light spectrum.

Fragmentation study of perovskite film $Cs_{0.2}(CH(NH_2)_2)_{0.8}PbI_3$ shows that the optimal cutting parameters for a nanosecond laser, namely a wavelength of 355 nm using power of 0.4 W and a scanning velocity of 110 mm/s, ensure perovskite patterning with a cell 'dead zone' width of 17 μm without damaging adjacent conducting layers.

Supplementary data

Supplementary data is available at *Clean Energy* online.

Acknowledgements

The authors gratefully acknowledge the financial support from the Ministry of Science and Higher Education of the Russian Federation in the framework of the Russian Science Foundation Grant No. 21-19-00853. R.I., P.G. and A.I. acknowledge the financial support of "Theoretical and methodological framework for digital transformation in radiology", (USIS No. 123031400118-0) in accordance with the Order No. 1196 dated December 21, 2022 "On approval of state assignments funded by means of allocations from the budget of the city of Moscow to the state budgetary (autonomous) institutions subordinate to the Moscow Health Care Department, for 2023 and the planned period of 2024 and 2025" issued by the Moscow Health Care Department.

Conflict of interest statement

The authors declare no competing interest.

Data Availability

The data underlying this article are available in the article and in its online supplementary material.

References

[1] Amat A, Mosconi E, Ronca E, *et al*. Cation-induced band-gap tuning in organohalide perovskites: interplay of spin-orbit coupling and octahedra tilting. *Nano Lett*, 2014, **14**:3608–3616.

[2] Stranks SD, Eperon GE, Grancini G, *et al*. Electron-hole diffusion lengths exceeding 1 micrometer in an organometal trihalide perovskite absorber. *Science*, 2013, **342**:341–344.

[3] Ishteev A, Constantinova K, *et al*. Investigation of structural and optical properties of $MAPbBr_3$ monocrystals under fast electrons irradiation. *J Mater Chem C*, 2022, **10**:5821–5828.

[4] Li N, Niu X, Chen Q, *et al*. Towards commercialization: the operational stability of perovskite solar cells. *Chem Soc Rev*, 2020, **49**:8235–8286.

[5] Chen Y, Yi HT, Wu X, *et al*. Extended carrier lifetimes and diffusion in hybrid perovskites revealed by Hall effect and photoconductivity measurements. *Nat Commun*, 2016, **7**:12253.

[6] Herz LM. Charge-carrier mobilities in metal halide perovskites: fundamental mechanisms and limits. *ACS Energy Lett*, 2017, **2**:1539–1548.

[7] National Renewable Energy Laboratory. *NREL Efficiency Chart*. https://www.nrel.gov/pv/cell-efficiency.html (5 April 2023, date last accessed).

[8] Ono LK, Park NG, Zhu K, *et al*. Perovskite solar cells towards commercialization. *ACS Energy Lett*, 2017, **2**:1749–1751. https://doi.org/10.1021/acsenergylett.7b00517

[9] Krüger O, Kang J-H, Spevak M, *et al*. Precision UV laser scribing for cleaving mirror facets of GaN-based laser diodes. *Appl Phys A*, 2016, **122**:396. https://doi.org/10.1007/s00339-016-9945-6

[10] Illy EK, Knowles M, Gu E, *et al*. Impact of laser scribing for efficient device separation of LED components. *Appl Surf Sci*, 2005, **249**:354–361. https://doi.org/10.1016/j.apsusc.2004.12.033

[11] Risch A, Hellmann R. Laser scribing of gallium doped zinc oxide thin films using picosecond laser. *Appl Surf Sci*, 2011, **258**:1849–1853. https://doi.org/10.1016/j.apsusc.2011.10.060

[12] Peelaers H, Kioupakis E, Van de Walle CG. Free-carrier absorption in transparent conducting oxides: phonon and impurity scattering in SnO_2. *Phys Rev B*, 2015, **92**:235201. https://doi.org/10.1103/PhysRevB.92.235201

[13] Königer T, Rechtenwald T, Al-Naimi I, *et al*. CO_2-laser treatment of indium tin oxide nanoparticle coatings on flexible polyethyleneterephthalate substrates. *J Coat Technol Res*, 2010, **7**:261–269. https://doi.org/10.1007/s11998-009-9181-5

[14] Yi J, Zhou H, Wei WH, *et al*. Micro-/nano-structures fabricated by laser technologies for optoelectronic devices. *Front Chem*, 2021, **9**:823715. https://doi.org/10.3389/fchem.2021.823715

[15] Wang X, Yu H, Li P, *et al*. Femtosecond laser-based processing methods and their applications in optical device manufacturing: a review. *Opt Laser Technol*, 2021, **135**:106687. https://doi.org/10.1016/j.optlastec.2020.106687

[16] Liang L, Ma T, Chen Z, *et al*. Patterning technologies for metal halide perovskites: a review. *Adv Mater Technol*, 2023, **8**:2200419. https://doi.org/10.1002/admt.202200419

[17] Yang M, Kim DH, Klein TR, *et al*. Highly efficient perovskite solar modules by scalable fabrication and interconnection optimization. *ACS Energy Lett*, 2018, **3**:322–328. https://doi.org/10.1021/acsenergylett.7b01221

[18] Egorov FS, Kukin AV, Terukov EI, *et al*. Improving the quality of laser scribing of transparent conductive oxide in the manufacture of thin-film solar modules. *J Tech Phys*, 2018, **88**:572–577. https://doi.org/10.21883/jtf.2018.04.45726.2346

[19] Palma AL, Matteocci F, Agresti A, *et al*. Laser-patterning engineering for perovskite solar modules with 95% aperture ratio. *IEEE J Photovoltaics*, 2017, **7**:1674–1680. https://doi.org/10.1109/JPHOTOV.2017.2732223

[20] Brooks KG, Nazeeruddin MK. Laser processing methods for perovskite solar cells and modules. *Adv Energy Mater*, 2021, **11**:2101149. https://doi.org/10.1002/aenm.202101149

[21] Schultz C, Fenske M, Dagar J, *et al*. Ablation mechanisms of nanosecond and picosecond laser scribing for metal halide perovskite module interconnection: an experimental and numerical analysis. *Sol Energy*, 2020, **198**:410–418. https://doi.org/10.1016/j.solener.2020.01.074

[22] Lin B-Q, Huang C-P, Tian K-Y, *et al*. Laser patterning technology based on nanosecond pulsed laser for manufacturing bifacial perovskite solar modules. *Int J Precis Eng Manuf Green Technol*, 2023, **10**:123–139. https://doi.org/10.1007/s40684-022-00421-3

[23] Gao Y, Liu C, Xie Y, *et al*. Can nanosecond laser achieve high-performance perovskite solar modules with aperture area efficiency over 21%? *Adv Energy Mater*, 2022, **12**:2202287. https://doi.org/10.1002/aenm.202202287

[24] Zhao J, Chai N, Chen X, *et al*. Nonthermal laser ablation of high-efficiency semitransparent and aesthetic perovskite solar cells. *Nanophotonics*, 2022, **11**:987–993. https://doi.org/10.1515/nanoph-2021-0683

[25] Wang C, Tan G, Luo X, *et al*. How to fabricate efficient perovskite solar mini-modules in lab. *J Power Sources*, 2020, **466**:228321. https://doi.org/10.1016/j.jpowsour.2020.228321

[26] Kondratenko V, Borisovsky V, Naumov A, *et al*. New technology of laser parallel thermocracking of brittle materials. *Opt Photon J*, 2013, **03**:6–10. https://doi.org/10.4236/opj.2013.32b002

[27] Saranin D, Komaricheva T, Luchnikov L, *et al*. Solar energy materials and solar cells hysteresis-free perovskite solar cells with compact and nanoparticle NiO for indoor application. *Sol Energy Mater Sol Cells*, 2021, **227**:111095. https://doi.org/10.1016/j.solmat.2021.111095

[28] Kondratenko V, Ishteev A, Ishteev R, Konstantinova K. Research of laser patterning of perovskite photo detector components. In: *Optical Technologies, Materials and Systems*, Moscow: Russian Federation, 2022, 102–107.